Supplemental Materials for

Optimization of a bacterial three-hybrid assay through *in vivo* titration of an RNA-DNA adapter protein

Clara D. Wang, Rachel Mansky, Hannah LeBlanc, Chandra M. Gravel, and Katherine E. Berry

This pdf file includes:

Supplemental Figures S1 to S6

Supplemental Tables S1 to S5

Supplemental References

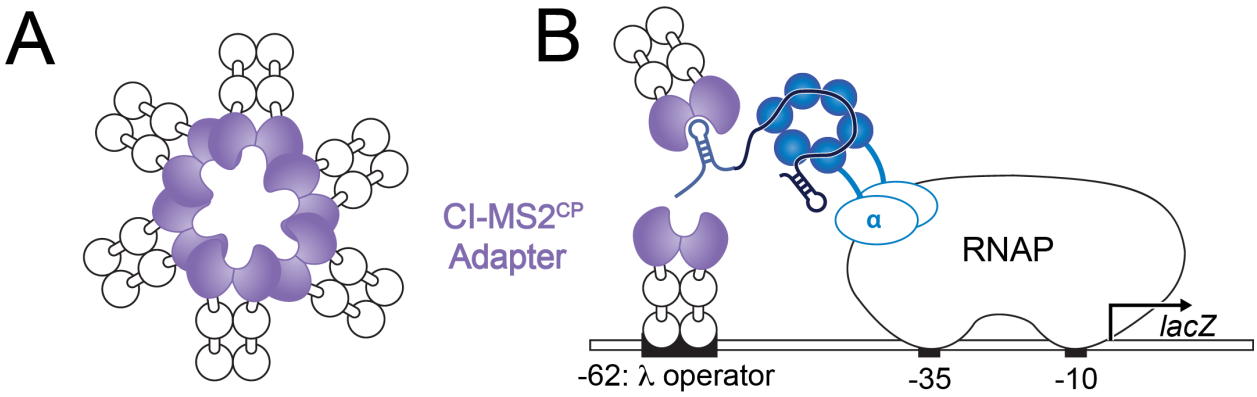

Supplemental Figure 1. Possible models for why B3H signal would be inhibited by high concentrations of adapter protein (CI-MS2^{CP}). (A) While we are using a multimerization-resistant version of MS2^{CP} (Macías et al. 2008), this component is still derived from a viral coat protein that has the potential to form large, higher-order assemblies in a concentration-dependent manner. It is possible that the adapter protein could multimerize at high concentrations through its MS2^{CP} moiety, in a way that blocks effective assembly of the B3H components. (B) Even in the absence of adapter multimerization, high concentrations of the adapter could inhibit B3H signal by "capping" hybrid RNAs. That is, if the adapter is present at high enough concentrations for one copy to bind the test promoter and a separate copy to bind the MS2^{hp} moiety of the hybrid RNA, the adapter would no longer serve as an effective bridge to stabilize RNAP at the test promoter.

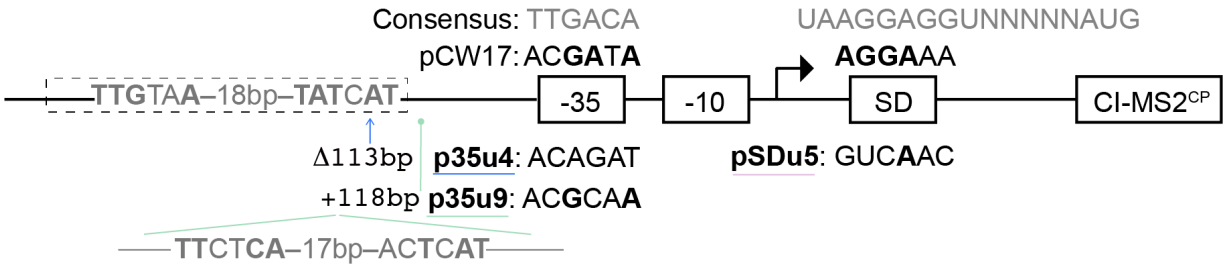

Supplemental Figure 2. Schematic depicting sequences of improved pAdapter constructs identified in forward genetic screen. The consensus sequence for *E. coli* σ^{70} promoter element (-35) along with the Shine-Dalgarno (SD) sequence are shown along the top in grey. The sequences for each of these elements in pCW17 are indicated above the line schematic. Matches to consensus are indicated with bold lettering. Below the line schematic are shown the sequences of three pAdapter constructs isolated from the pCW17-derived mutagenesis library (p35u4, p35u9 isolated from a plasmid library in which the -35 region was mutated and pSDu5 from one in which the Shine Dalgarno element was mutated). Regions of these plasmids in which the sequence differs from the parental pCW17 sequence are shown. Matches to consensus are indicated with bold lettering. pSDu5 only differed from pCW17 in the SD region, whereas p35u4 and p35u9 differed from pCW17 in the -35 region, as well as in an upstream deletion (Δ113bp; p35u4) or insertion (+118bp; p35u9) relative to pCW17. σ^{70} promoter matches in the deleted region (dashed box) or in the inserted region are shown.

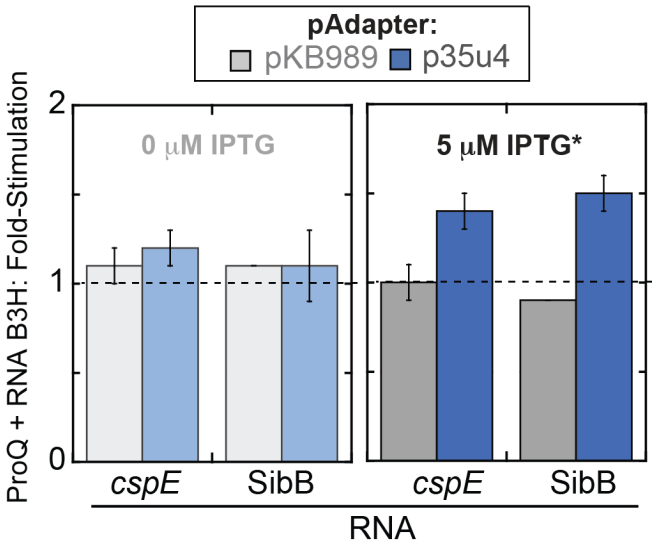

Supplemental Figure 3. Results of β-gal B3H assays between RNAs and ProQ. Assays were conducted in KB483 cells grown in presence or absence of 5 uM IPTG*, with pAdapter (CI-MS2^{CP} fusion expressed from pKB989 or p35u4), pPrey (α-ProQ, pKB949) and pBaitRNA (1xMS2^{hp}-*cspE*, pSP10 or 1xMS2^{hp}-SibB, pSP14). The bar graph shows the fold-stimulation over basal levels: that is, the β-gal activity measured in the presence of all hybrid constructs divided by the activity of the highest negative control sample expressing only half of one hybrid construct. The dashed horizontal line represents “basal” levels. Data are presented as the average value of three independent measurements and error bars show the standard deviation of these values.

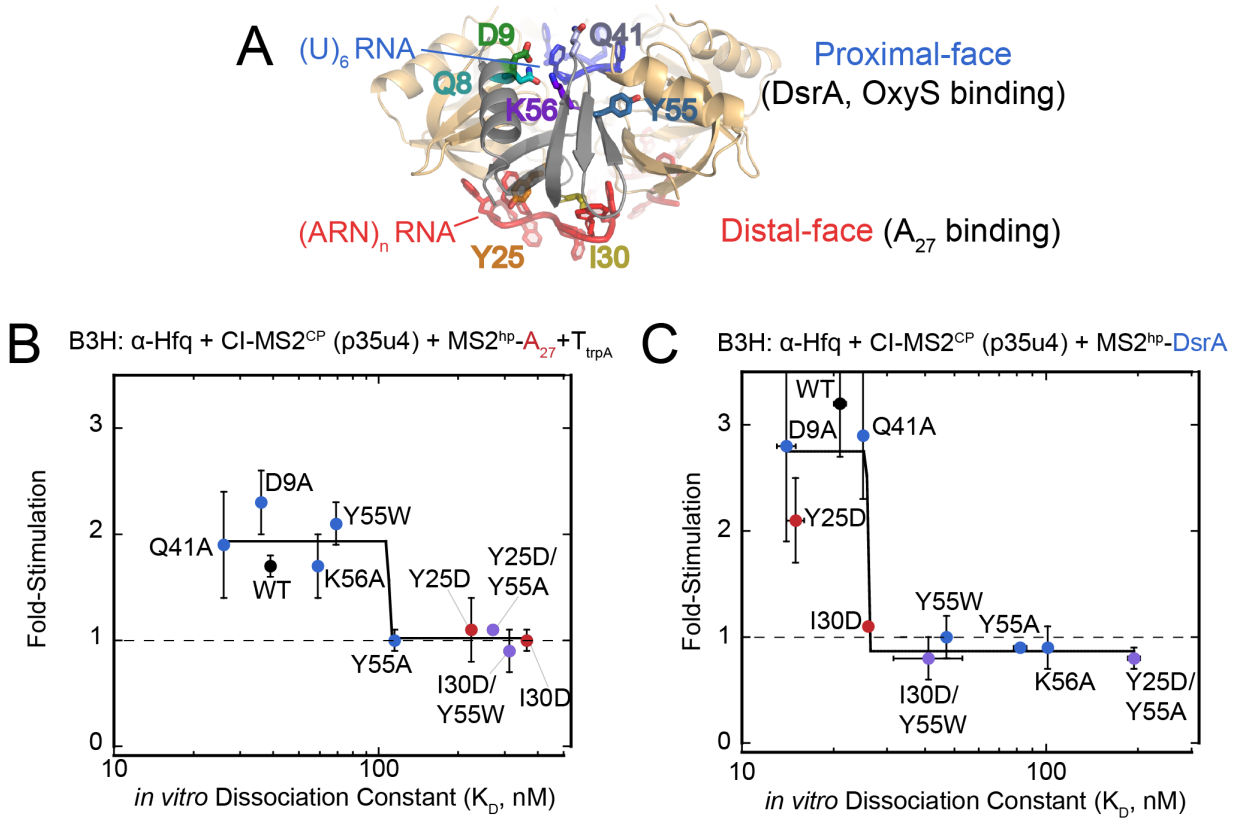

Supplemental Figure 4. Location of Hfq residues targeted for mutagenesis. (A) Crystal structure of Hfq hexamer, bound to poly(U) and poly(A) RNA on the proximal and distal faces, respectively (PDB ID = 4HT9) (Wang et al. 2013). One hexamer is shown as a grey cartoon; the side chains of residues targeted for mutagenesis are shown on this grey monomer in stick representation. (B,C) Results of β-gal B3H assays between A_{27} and DsrA RNAs and Hfq mutants. Assays were conducted in KB483 cells grown in presence of 5 uM IPTG*, with pAdapter (p35u4), pPrey (α-Hfq; WT or indicated variant) and pBaitRNA (2x$MS2^{hp}$-DsrA, pHL34 or 1x$MS2^{hp}$-A_{27}-T_{trpA}, pHL26). Fold-stimulation for B3H assays between both RNA and each Hfq variant was plotted against the K_D value determined previously for each interaction using gel-shift assays (Mikulecky et al. 2004). Data for (B) A_{27} and (C) DsrA from Figure 7C are plotted on separate axes with each individual Hfq mutant labeled. Data points are colored based on the surface of Hfq that is affected by the mutation (red = distal; blue = proximal; purple = double mutant with substitutions on both faces).

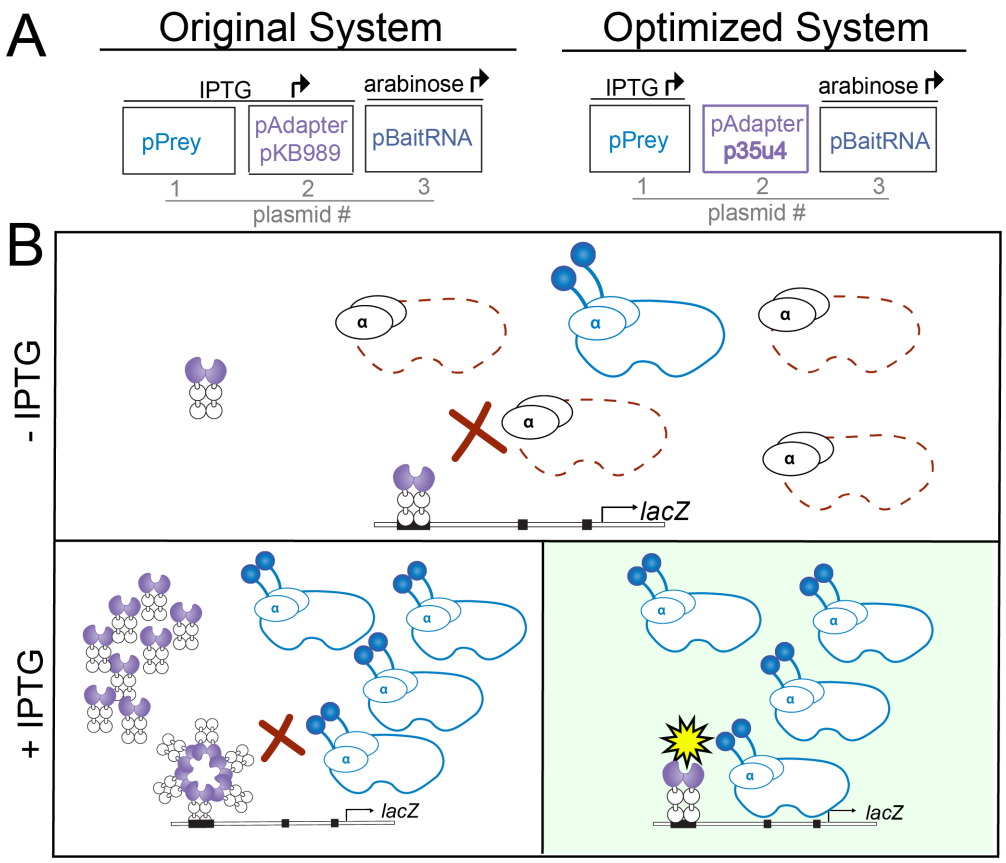

Supplemental Figure 5. Model for how a constitutive pAdapter, such as p35u4, improves B3H assay signal. (A) Schematic showing the plasmids used to express prey, adapter, and bait hybrid components in the original vs. optimized B3H system, along with inducers that drive expression of each component. The key difference is that adapter protein was originally induced by IPTG along with prey protein; in the optimized system, adapter concentration is fixed through a constitutive pAdapter construct, and the concentration of prey fusion protein can be modulated independently. (B) Depiction of relative concentrations of assay components in the absence (top) or presence (bottom) of IPTG when assay is conducted with original pAdapter (IPTG-inducible, pKB989, left) or with optimized pAdapter (constitutive, p35u4, right). In the absence of IPTG, both prey and adapter proteins are expressed at low levels (through leaky and/or constitutive expression). Signal is limited by the low concentration of prey fusion protein, such that most RNAP molecules in the cell are not displaying the prey fusion protein (shown as dashed red outlines). In the presence of IPTG, more prey fusion protein is expressed, leading to more RNAP molecules displaying prey (shown in blue). However, high concentrations of the adapter are also achieved in the original system, which may inhibit B3H signal (see Fig S1). In the optimized system and in the presence of IPTG (bottom, right), adapter expression is kept low while prey expression is high, leading to optimal signal.

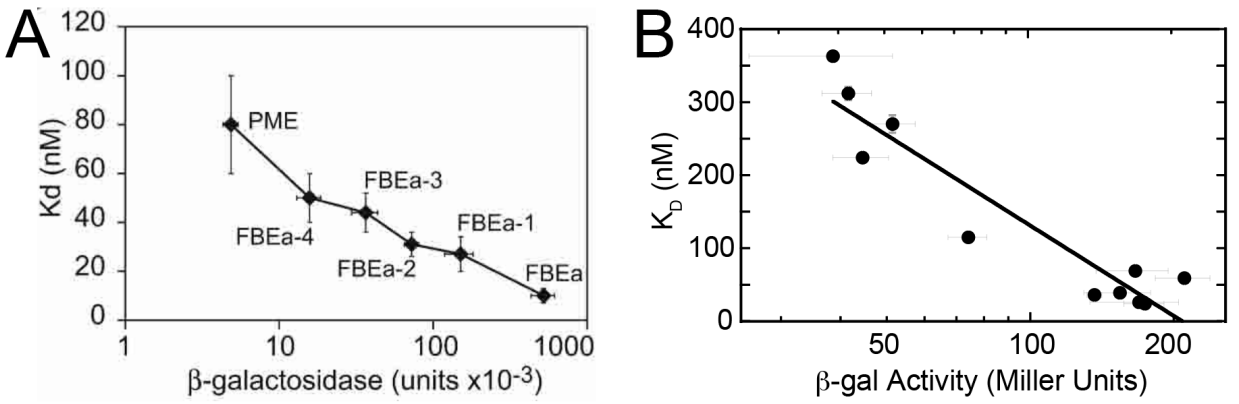

Supplemental Figure 6. Comparison of relationship between *in vitro* binding affinities and genetic signal in yeast three-hybrid (Y3H) and B3H systems. (A) Panel is reproduced from Hook et al. 2005. Comparison of *in vitro* binding affinities measured by gel-shift assays to Y3H reporter gene activation in YBZ1 for interactions between the PUF protein FBF-1 and six RNAs (Hook et al. 2005). (B) Data from Figure 7C plotted in the same manner as Y3H data in (A). Results of β-gal B3H assays between A_{27} RNA and Hfq mutants conducted in KB483 cells grown in presence of 5 uM IPTG* with pAdapter (p35u4), pPrey (α-Hfq; WT or indicated variant) and pBaitRNA (1xMS2^{hp}-A27-T_{trpA}, pHL26). The K_D value for interaction between A_{27} RNA and each Hfq variant — determined previously using gel-shift assays (Mikulecky et al. 2004) — was plotted against raw β-gal value activity measured for each interaction, plotted on a logarithmic scale. Data are fit to the logarithmic function y=a+b*log(x), R=0.94.

SUPPLEMENTAL TABLES

Table S1. *E. coli* strains used in this study.

Strain	Genotype	Antibiotic Resistance	Source	Figures
NEB 5α- F'I^q Competent E. coli	*E. coli* host strain for plasmid construction*: F´ proA$^+$B$^+$ lacI^q Δ(lacZ)M15 zzf::Tn10 (Tet^R) / fhuA2Δ(argF lacZ)U169 phoA glnV44 Φ80Δ(lacZ)M15 gyrA96 recA1 relA1 endA1 thi-1 hsdR17*	TetR	New England Biolabs	[used for cloning]
KB473	FW102 *Δhfq*::FRT harboring F' episome bearing kanamycin resistance and test promoter *placO$_L$2-62* fused to *lacZ*	KanR; StrR	(Berry and Hochschild 2018)	Fig 1, 2A, Fig 3, Fig 5, Fig 6
KB483	FW102 *hfq::kan* harboring F' episome bearing tetracycline resistance and test promoter *placO$_L$2-62* fused to *lacZ*	TetR; StrR	(Pandey et al. 2020)	Fig 2B, Fig 7
FW123	FW102 harboring F' episome bearing kanamycin resistance and a *lacZ* reporter gene controlled by a promoter harboring the λCI operator positioned between the - 35 and -10 elements.	KanR	(Pinkett et al. 2006; Whipple et al. 1994)	Fig 3B,C,E,F; Fig 4D,F; Fig 5A,B

Table S2. Plasmids used in this study

Name	Description	Details	Antibiotic Resistance	Reference/ Source	Figures
pACλCI	pACλCI-empty vector	Encodes full length λCI under control of *lacUV5* promoter. p15A origin of replication.	CmR	(Berry and Hochschild 2018)	through out
pACλCI-β-flap	pACλCI-β-flap$^{831\text{-}1057}$	P_{lacUV5} -directed synthesis of the λCI protein fused via three alanines to residues 831-1057 of the β subunit of *E. coli* RNAP. p15A origin of replication.	CmR	(Deighan et al. 2008)	Fig 2B
pACΔCI	pAC-empty vector	Comparable to pACλCI but lacking λCI ORF following *lacUV5* promoter	CmR	(Pinkett et al. 2006; Whipple et al. 1994)	Fig 3C,E; 4D,F
pBRα	pBr-α-empty vector	Encodes residues 1-248 of the alpha vector fused under control of *lpp* and *lacUV5* promoters. pBR322 origin of replication.	AmpR	(Berry and Hochschild 2018)	through out
pBR-σ^{70}	pBR-σ70^{D581G}	P_{lacUV5} /P_{lpp} -directed synthesis of the λCI protein fused directly to *E. coli* σ^{70} region 4 (residues 528-613 of σ^{70}). The σ^{70} moiety also carries the D581G substitution. pBR322 origin of replication.	AmpR	(Kuznedelov et al. 2002)	Fig 2B
pCH1	pCDF-pBAD-1xMS2^{hp}	Encodes a single MS2^{hp} under the control of an arabinose-inducible promoter, followed by XmaI and HindIII sites. CloDF13 origin of replication.	SpecR	(Pandey et al. 2020)	Fig S3
pCH9	pCDF-pBAD-1xMS2^{hp}-OxyS	*E. coli oxyS* inserted into pCH1 following 1xMS2^{hp} between XmaI and HindIII sites; intrinsic terminator encoded by sRNA.	SpecR	(Pandey et al. 2020)	Fig 7B
pCW14	pAC-$p_{constit}$-CI-MS2	Encodes CI-MS2^{CP} fusion protein under the control of a constitutive promoter. Comparable to pCW18 (Δ*lacO*) but with -35: ACGATA and -10 TATACT	CmR	This study (oCW28 + oCW29 + oCW30 + oCW31)	Fig 3E,F; 5A
pCW15	pAC-$p_{constit}$-CI-MS2	Encodes CI-MS2^{CP} fusion protein under the control of a constitutive promoter. Comparable to pCW18 (Δ*lacO*) but with -35: CCGATA and -10 TATACT	CmR	This study (oCW30 + oCW31)	Fig 3E,F; 5A
pCW16	pAC-$p_{constit}$-CI-MS2	Encodes CI-MS2^{CP} fusion protein under the control of a constitutive promoter. Comparable to pCW18	CmR	This study (oCW32 + oCW33+	Fig 3E,F; 5A

		(Δ*lacO*) but with -35: CCGACA and -10 TATACT		oCW30 + oCW31)	
pCW17	pAC-$p_{constit}$-CI-MS2	Encodes CI-$MS2^{CP}$ fusion protein under the control of a constitutive promoter. Comparable to pCW18 (Δ*lacO*) but with -35: ACGATA and -10 TATAGT. p15A origin of replication.	CmR	(Pandey et al. 2020)	Fig 3E,F; 4B, C, D, F; 5A,B; 7B
pCW18	pAC-$p_{constit}$-CI-MS2	Encodes CI-$MS2^{CP}$ fusion protein under the control of a constitutive promoter. Relative to *lacUV5* promoter in pKB989, Δ*lacO*, -35: CCGACA, -10 TATAGT. p15A origin of replication.	CmR	This study; oCW32 + oCW33)	Fig 3C,D,E, F; 5A
pCW19	pAC-$p_{constit}$-CI-MS2	Encodes CI-$MS2^{CP}$ fusion protein under the control of a constitutive promoter. Comparable to pCW18 (Δ*lacO*) but with -35: CCGATA and -10 GATAGT	CmR	This study (oCW34 + oCW35	Fig 3E,F; 5A
pCW24	pAC-$p_{constit}$-CI-MS2-Δpromoter	Comparable to pCW17, encodes the CI-$MS2^{CP}$ fusion protein, but 30bp which encoded the constitutive promoter (-10 to -35 elements) have been deleted.	CmR	This study (oCW45 + oCW46 on pCW17)	Fig 4F
pHL6	pCDF-pBAD-1x$MS2^{hp}$-T_{trpA}	Intrinsic terminator from *trpA* operon cloned behind $MS2^{hp}$ and HindIII site in pCH1; under the control of an arabinose-inducible promoter; CloDF13 origin of replication.	SpecR	(Pandey et al. 2020)	Fig 7C, D; S4; S6
pHL23	pBr-α-Ec-Hfq-I30D	*hfq* I30D mutation introduced to pKB817 by PCR.	AmpR	This study (oHL52 + oHL53)	Fig 7A-D
pHL26	pCDF-pBAD-1x$MS2^{hp}$-A_{27}-T_{trpA}	poly(A) sequence of 27 adenosine nucleotides cloned behind $MS2^{hp}$ between XmaI/HindIII residues in pHL6; transcriptional termination provided by *trpA* terminator; under the control of an arabinose-inducible promoter; CloDF13 origin of replication.	SpecR	This study (oHL54 + oHL55 into pHL6)	Fig 7C, D; S4; S6
pHL34	pCDF-pBAD-2x$MS2^{hp}$-ΔXmaI-DsrA	*E. coli dsrA* inserted into pKB845 following 2x$MS2^{hp}$ between XmaI and HindIII sites; XmaI site removed by PCR; intrinsic terminator encoded by sRNA	SpecR	This study (oHL62 + oHL63 on pKB941)	Fig 7C; S4C
pHL54	pBr-α-Ec-Hfq-D9A	*hfq* D9A mutation introduced to pKB817 by PCR.	AmpR	This study (oHL88 + oHL89)	Fig 7A,C,D; S4

pHL58	pBr-α-Ec-Hfq-Q41A	*hfq* Q41A mutation introduced to pKB817 by PCR.	AmpR	This study (oHL9 6+ oHL97)	Fig 7A,C,D; S4
pHL60	pBr-α-Ec-Hfq-Y55W	*hfq* Y55W mutation introduced to pKB817 by PCR.	AmpR	This study (oHL100 + oHL101)	Fig 7A,C,D; S4
pHL61	pBr-α-Ec-Hfq-Y25D-Y55A	*hfq* Y25D and Y55A mutations introduced to pKB817 by PCR.	AmpR	This study (oHL102 + oHL103)	Fig 7A,C,D; S4
pHL63	pBr-α-Ec-Hfq-I30D-Y55W	*hfq* I30D and Y55W mutations introduced to pKB817 by PCR.	AmpR	This study (oHL100 + oHL101)	Fig 7A,C,D; S4
pKB815	pBr-α-MS2^{CP}	Encodes residues 1-248 of alpha fused via three alanine residues to MS2 coat protein with following mutations to avoid multimerization: V30I, A81G, positions 68-80 deleted (VATQTVGGVELPV). Analogous to pKB994 (Berry and Hochschild 2018), but with a shorter linker. pBR322 origin of replication.	AmpR	This study (oKB1038 + oKB1039)	Fig 2B
pKB816	pACλCI-Hfq	Encodes residues 1-236 of λCI fused via three alanine residues to full-length wild-type *E.coli* Hfq.	CmR	(Berry and Hochschild 2018)	Fig 1E; 7A
pKB817	pBr-α-Hfq	Encodes residues 1-248 of alpha vector linked to full-length wild-type *E. coli* Hfq via three alanine residues; inserted into pBRα between NotI and BamHI sites; pBR322 origin of replication.	AmpR	(Berry and Hochschild 2018)	Fig 1D-F; 3D,F; 4B,C; 5A-C; 6A-B; 7A-D; S4; S6
pKB845	pCDF-pBAD-2xMS2^{hp}	Two MS2 hairpins (2xMS2^{hp}) and an XmaI site inserted into pKB822 CDF origin vector between BamHI and HindIII sites. under the control of an arabinose-inducible promoter; CloDF13 origin of replication.	SpecR	(Berry and Hochschild 2018)	through out
pKB854	pCDF-pBAD-2xMS2^{hp}-SgrS	*E. coli sgrS* inserted into pKB845 following 2xMS2^{hp} between XmaI and HindIII sites; intrinsic terminator encoded by sRNA	SpecR	This study (oKB1107 + oKB1108)	Fig 1F; Fig 6
pKB856	pCDF-pBAD-2xMS2^{hp}-MgrR	*E. coli mgrR* inserted into pKB845 following 2xMS2^{hp} between XmaI and HindIII sites; intrinsic terminator encoded by sRNA	SpecR	(Berry and Hochschild 2018)	Fig 1F; 4B,C; 5A,C; Fig 6

pKB872	pBr-α-Ec-Hfq-Y55A	*hfq* Y55A mutation introduced to pKB817 by PCR	AmpR	This study (oKB1117 + oKB1118)	Fig 7A,C,D; S5
pKB873	pBr-α-Ec-Hfq-K56A	*hfq* K56A mutation introduced to pKB817 by PCR	AmpR	This study (oKB1119 + oKB1120)	Fig 7A-D; S4
pKB905	pBr-α-Ec-Hfq-Y25D	*hfq* Y25D mutation introduced to pKB817 by PCR	AmpR	This study (oKB1186 + oKB1187)	Fig 7A-D; S4
pKB909	pCDF-pBAD-2xMS2^{hp}-ChiX	*E. coli chiX* inserted into pKB845 following 2xMS2^{hp} between XmaI and HindIII sites; intrinsic terminator encoded by sRNA	SpecR	(Berry and Hochschild 2018)	Fig 1D,F; 5B-C; Fig 6
pKB910	pCDF-pBAD-2xMS2^{hp}-McaS	*E. coli mcaS* inserted into pKB845 following 2xMS2^{hp} between XmaI and HindIII sites; intrinsic terminator encoded by sRNA	SpecR	(Berry and Hochschild 2018)	Fig 1F; Fig 6
pKB911	pCDF-pBAD-2xMS2^{hp}-CyaR	*E. coli cyaR* inserted into pKB845 following 2xMS2^{hp} between XmaI and HindIII sites; intrinsic terminator encoded by sRNA	SpecR	This study (oKB1194 + oKB1195)	Fig 1F; Fig 6
pKB912	pCDF-pBAD-2xMS2^{hp}-OxyS	*E. coli oxyS* inserted into pKB845 following 2xMS2^{hp} between XmaI and HindIII sites; intrinsic terminator encoded by sRNA	SpecR	(Berry and Hochschild 2018)	Fig 1F; Fig 6; 7B
pKB913	pCDF-pBAD-2xMS2^{hp}-RyhB	*E. coli ryhB* inserted into pKB845 following 2xMS2^{hp} between XmaI and HindIII sites; intrinsic terminator encoded by sRNA	SpecR	(Berry and Hochschild 2018)	Fig 1F; Fig 6
pKB941	pCDF-pBAD-2xMS2^{hp}-DsrA	*E. coli dsrA* inserted into pKB845 following 2xMS2^{hp} between XmaI and HindIII sites; intrinsic terminator encoded by sRNA	SpecR	This study (oKB1209 + oKB1210)	n/a (cloning interme diate)
pKB942	pCDF-pBAD-2xMS2^{hp}-ArcZ	*E. coli arcZ* inserted into pKB845 following 2xMS2^{hp} between XmaI and HindIII sites; intrinsic terminator encoded by sRNA	SpecR	This study (oKB1211 + oKB1212)	Fig 1F; Fig 6
pKB949	pBRα-ProQ^{FL}	Encodes residues 1-248 of alpha vector fused via three alanine residues to full-length wild-type *E. coli proQ;* inserted into pBRα between NotI and BamHI sites; pBR322 origin of replication	AmpR	(Pandey et al. 2020)	Fig S3
pKB989	pACλCI-MS2^{CP}	Encodes residues 1-236 of CI fused to MS2 coat protein (MS2^{CP}) via three alanine residues; includes mutations V30I, A81G, and deletion of residues 68-80 in order to avoid multimerization. This fusion protein	CmR	(Berry and Hochschild 2018)	Fig 1D,E,F; Fig 2; 3C,D,E; 4C,D;

		is expressed under control of a *lacUV5* promoter.			Fig 6; 7B
pRM24	pAC-$p_{constit*}$-CI-MS2-Δpromoter	Comparable to p35u4, encodes the CI-$MS2^{CP}$ fusion protein, but 30bp which encoded the constitutive promoter (-10 to -35 elements) have been deleted.	CmR	This study (oCW45 + oRM35)	Fig 4F
pSP10	pCDF-1XMS2^{hp}-*cspE*3'UTR	*E. coli* 3' UTR of *cspE* inserted into pCH1 following 1xMS2^{hp} between XmaI and HindIII sites; intrinsic terminator encoded by sRNA	SpecR	(Pandey et al. 2020)	Fig S3
pSP14	pCDF-1XMS2^{hp}-SibB	*E. coli sibB* inserted into pCH1 following 1xMS2^{hp} between XmaI and HindIII sites; intrinsic terminator encoded by sRNA	SpecR	(Pandey et al. 2020)	Fig S3
p35u4	pAC-$p_{constit*}$-CI-MS2	Encodes CI-$MS2^{CP}$ fusion protein under control of a constitutive promoter; p15A origin of replication. Isolated from a pCW17-derived mutagenesis library. See Fig S3 for changes relative to pCW17.	CmR	This study (forward genetic screen)	Fig 4C,D,F; 5; 6; 7B-D; S3; S4; S6
p35u9, pSDu5	pAC-$p_{constit}$-CI-MS2				Fig 5

Table S3. Oligonucleotides used in the study. QC indicates primers used for Quikchange-style mutagenesis; Q5 indicates primers designed with NEBBase changer for Q5 Site-Directed Mutagenesis.

Name	**Description**	**Used for**	**Sequence**
oCW5	F pAdapter	Sequencing primer	CAGACCAAAACGATCTCAAGAAGATCATC
oCW28	F -35 ACGATA	QC PCR: pCW14, 17	CCAGGCCTCGAGACGATAGCTAGCTCAGTC
oCW29	R -35 ACGATA	QC PCR: pCW14, 17	GACTGAGCTAGCTATCGTCTCGAGGCCTGG
oCW30	F -10 TATACT	QC PCR: pCW14, 15, 16	GCTCAGTCCTAGGTATACTGCTAGCGCATGCC
oCW31	R -10 TATACT	QC PCR: pCW14, 15, 16	GGCATGCGCTAGCAGTATACCTAGGACTGAGC
oCW32	F -35 CCGACA	QC PCR: pCW16, 18	CAGGCCTCGAGCCGACAGCTAGCTCAGT
oCW33	R -35 CCGACA	QC PCR: pCW16, 18	ACTGAGCTAGCTGTCGGCTCGAG CCTG

oCW34	F -10 GATAGT	QC PCR: pCW19	GCTCAGTCCTAGGGATAGTGCTAGCGCATGCC
oCW35	R -10 GATAGT	QC PCR: pCW19	GGCATGCGCTAGCACTATCCCTAGACTGAGC
oCW22	F -35 CCGATA	QC PCR: pCW 15,19	CAGGCCTCGAGCCGATAGCTAGCTCAGTC
oCW23	R -35 CCGATA	QC PCR: pCW 15,19	GACTGAGCTAGCTATCGGCTCGAGGCCTG
oCW36	F -35 library	Q5 PCR: -35 library	AGGCCTCGAGNNNNNNGCTAGCTCAGTCCTAGG
oCW37	R -35 library	Q5 PCR: -35 library	GGGGTGCCTAATGAGTGA
oCW40	F SD library	Q5 PCR: SD library	CATGCCACACNNNNNNCAGCGTATGAGC
oCW41	R SD library	Q5 PCR: SD library	CGCTAGCACTATACCTAG
oHL52	F Hfq I30D	Q5 PCR: pHL24	GGTGAATGGTGACAAGCTGCAAG
oHL54	F A_{27}	Q5 PCR: pHL26	AAAAAAAAAAAAAAAAAAAAGCTTAGCCCGCCTAATGAG
oHL55	R A_{27}	Q5 PCR: pHL26	TTTTTTTTCCCGGGCTGCAGACATGG
oHL58	R Hfq I30D	Q5 PCR: pHL24	AAATAAATAGAAACTGGAACAC
oHL62	F DsrA ΔXmaI	Q5 PCR: pHL34	AACACATCAGATTTCCTGG
oHL63	R DsrA ΔXmaI	Q5 PCR: pHL34	CTGCAGACATGGGTGATC
oHL88	F Hfq D9A	Q5 PCR: pHL54	TCTTTACAAGCTCCGTTCCTGAACGCAC
oHL89	R Hfq D9A	Q5 PCR: pHL54	TTGCCCCTTAGCTGCGGC
oHL96	F Hfq Q41A	Q5 PCR: pHL58	GTCTTTTGATGCGTTCGTGATCCTGTTGAAAAAC
oHL97	R Hfq Q41A	Q5 PCR: pHL58	TCGATTTGCCCTTGCAGC
oHL100	F Hfq Y55W	Q5 PCR: pHL60/63	CCAGATGGTTTGGAAGCACGCGA
oHL101	R Hfq Y55W	Q5 PCR: pHL60 + pHL63	CTGACCGTGTTTTTCAAC
oHL102	F Hfq Y55A	Q5 PCR: pHL61	CCAGATGGTTGCCAAGCACGCGA
oHL103	R Hfq Y55A	Q5 PCR: pHL61	CTGACCGTGTTTTTCAACAG
oRM20	R Seq pAdapter	Sequencing primer	GCTTTAAGGCGACGTGCGTCC
oKB1038	F NotI $MS2^{CP}$	PCR: pKB815	ATAAGAATGCGGCCGCAGCTTCTAACTTTACTCAGTTCGTTCTCG
oKB1039	R BamHI $MS2^{CP}$	PCR: pKB815	CTTCGGATCCTTAGTAGATGCCGGAGTTTGCTGC
oKB1117	F Hfq Y55A	QC PCR: pKB872	GTCAGCCAGATGGTTGCCAAGCACGCGATTTC

oKB1118	R Hfq Y55A	QC PCR: pKB872	GAAATCGCGTGCTTGGCAACCATCTGGCTGAC
oKB1119	F Hfq K56A	QC PCR: pKB873	CAGCCAGATGGTTTACGCGCACGCGATTTCTAC
oKB1120	R Hfq K56A	QC PCR: pKB873	GTAGAAATCGCGTGCGCGTAAACCATCTGGCTG
oKB1186	F Hfq Y25D	QC PCR: pKB905	CGTGTTCCAGTTTCTATTGATTTGGTGAATGGTATTAAGC
oKB1187	R Hfq Y25D	QC PCR: pKB905	GCTTAATACCATTCACCAAATCAATAGAAACTGGAACACG
oKB1209	F DsrA XmaI	PCR: pKB941	TCCCCCCGGGAACACATCAGATTTCCTGGTGTAAC
oKB1210	R DsrA HindIII	PCR: pKB941	CCGGCCAAGCTTAAAAAAAATCCCGACCCTGAGGG
oKB1211	F ArcZ XmaI	PCR: pKB942	TCCCCCCGGGGTGCGGCCTGAAAAACAGTGC
oKB1212	R ArcZ HindIII	PCR: pKB942	CCGGCCAAGCTTAAAAAATGACCCCGGCTAGACC
oKB1194	F CyaR XmaI	PCR: pKB911	TCCCCCCGGGGCTGAAAAACATAACCCATAAAATGCTAGC
oKB1195	R CyaR HindIII	PCR: pKB911	CCGGCCAAGCTTAAAAAATAAGCCCGTGTAAGGGAGATTAC
oKB1109	F MgrR XmaI	PCR: pKB856	TCCCCCCGGGGATTCGTTATCAGTGCAGGAAAATGCC
oKB1110	R MgrR HindIII	PCR: pKB856	CCGGCCAAGCTTAAAAAAAACCGCCAGTAAACCGGC

Table S4. Predicted constitutive promoter strengths in pAdapter constructs generated by site-directed mutagenesis. The -35 and -10 sequences are provided for each plasmid; bold letters represent a match to the σ^{70} consensus sequence. Plasmids are arranged in order of decreasing predicted strength as determined using the energy binding matrix determined in Brewster et al. 2012.

Plasmid	Promoter sequence (-35)	(-10)	Relative Strength
Consensus	**TTGACA**	**TATAAT**	3.7 (strongest)
pKB989 fully de-repressed	**TT**T**ACA**	**TATAAT**	2.7 *
pKB989 fully repressed (leaky expression)			< 2.7 **
pCW14	AC**GA**T**A**	**TATA**C**T**	2.2
pCW15	CC**GA**T**A**	**TATA**C**T**	1.9
pCW16	CC**GA**C**A**	**TATA**C**T**	1.8
pCW17	AC**GA**T**A**	**TATA**G**T**	1.8
pCW18	CC**GA**C**A**	**TATA**G**T**	1.3
pCW19	CC**GA**T**A**	G**ATA**G**T**	1.2 (weakest)

* pKB989 encodes the CI-MS2^{CP} fusion protein under the control of an IPTG-inducible *lacUV5* promoter. The value listed above is the predicted strength of the fully de-repressed promoter in the absence of any LacI repression.

** When pKB989 is fully repressed (in the absence of IPTG), there is some leaky expression, but this cannot be predicted from the energy binding matrix.

Table S5. Dissociation constants for Hfq-sRNA interactions for Hfq mutants from literature.

	Dissociation Constant (K_D; nM)				
Hfq variant	**A_{27}[1]**	**DsrA[1]**	**OxyS[2]**	**A_{27}[2]**	**DsrA[2]**
WT	39 ± 1	32 ± 1	1.7 ± 1.1	.87 ± .35	.74 ± .4
D9A	36 ± 1	14 ± 1			
Y25D	224 ± 2	15 ± 1	3.5 ± 1.6	> 250	1.4 ± .13
I30D	363 ± 3	26 ± 1	5.9 ± 2.3	> 250	2.1 ± 1.2
Q41A	26 ± 1	25 ± 1			
Y55A	115 ± 2	82 ± 4			
Y55W	69 ± 1	47 ± 1			
K56A	59 ± 1	101 ± 2	100 ± 20	6.8 ± 3.1	180 ± 62
I30D/Y55W	312 ± 9	41 ± 12			
Y25D/Y55A	270 ± 12	194 ± 9			

[1] K_D values measured by gel-shift assays and reported in (Mikulecky et al. 2004).
[2] K_D values measured by filter-binding assays and reported in (Olejniczak 2011).

SUPPLEMENTAL REFERENCES

Berry KE, Hochschild A. 2018. A bacterial three-hybrid assay detects *Escherichia coli* Hfq-sRNA interactions in vivo. *Nucleic Acids Res* **46**: e12.

Brewster RC, Jones DL, Phillips R. 2012. Tuning promoter strength through RNA polymerase binding site design in *Escherichia coli*. *PLoS Comput Biol* **8**: e1002811.

Deighan P, Diez CM, Leibman M, Hochschild A, Nickels BE. 2008. The bacteriophage λ Q antiterminator protein contacts the β-flap domain of RNA polymerase. *Proc Natl Acad Sci U S A* **105**: 15305–15310.

Hook B, Bernstein D, Zhang B, Wickens M. 2005. RNA-protein interactions in the yeast three-hybrid system: affinity, sensitivity, and enhanced library screening. *RNA* **11**: 227–233.

Kuznedelov K, Minakhin L, Niedziela-Majka A, Dove SL, Rogulja D, Nickels BE, Hochschild A, Heyduk T, Severinov K. 2002. A role for interaction of the RNA polymerase flap domain with the sigma subunit in promoter recognition. *Science* **295**: 855-857.

Macías S, Bragulat M, Tardiff DF, Vilardell J. 2008. L30 binds the nascent RPL30 transcript to repress U2 snRNP recruitment. *Mol Cell* **30**: 732–742.

Mikulecky PJ, Kaw MK, Brescia CC, Takach JC, Sledjeski DD, Feig AL. 2004. *Escherichia coli* Hfq has distinct interaction surfaces for DsrA, rpoS and poly(A) RNAs. *Nat Struct Mol Biol* **11**: 1206–1214.

Olejniczak M. 2011. Despite similar binding to the Hfq protein regulatory RNAs widely differ in their competition performance. *Biochemistry* **50**: 4427–4440.

Pandey S, Gravel CM, Stockert OM, Wang CD, Hegner CL, LeBlanc H, Berry KE. 2020. Genetic identification of the functional surface for RNA binding by *Escherichia coli* ProQ. *Nucleic Acids Res* **48**: 4507–4520.

Pinkett HW, Shearwin KE, Stayrook S, Dodd IB, Burr T, Hochschild A, Egan JB, Lewis M. 2006. The structural basis of cooperative regulation at an alternate genetic switch. *Mol Cell* **21**: 605–615.

Wang W, Wang L, Wu J, Gong Q, Shi Y. 2013. Hfq-bridged ternary complex is important for translation activation of rpoS by DsrA. *Nucleic Acids Res* **41**: 5938–5948.

Whipple FW, Kuldell NH, Cheatham LA, Hochschild A. 1994. Specificity determinants for the interaction of lambda repressor and P22 repressor dimers. *Genes Dev* **8**: 1212–1223.